Title:

Comparative assessment of condensation and pool boiling heat transfer on horizontal plain single tubes for R1234ze(E), R1234ze(Z), and R1233zd(E)

Authors:

Ryuichi Nagata [1], Chieko Kondou [2], Shigeru Koyama [1, 3]

Affiliations:

1, Interdisciplinary Graduate School of Engineering Sciences, Kyushu University, 6-1 Kasuga-koen, Kasuga, Fukuoka 816-8580, Japan

2, Graduate School of Engineering, Nagasaki University, 1-14 Bunkyo, Nagasaki, 852-8521, Japan

3, International Institute for Carbon-Neutral Energy Research (WPI-I^{2}CNER), Kyushu University, 6-10-1, Hakozaki, Higashi-ku, Fukuoka, 812-8581, Japan

* Corresponding author.

Tel.: +81 95 819 2527

E-mail address: ckondou@nagasaki-u.ac.jp (C. Kondou)

ABSTRACT

The low-global warming potential (GWP) refrigerant of R1234ze(E) is considered to be a prospective alternative to conventional R134a for car air conditioners, whereas the isomer R1234ze(Z) and R1233zd(E) are anticipated to be the low-GWP alternatives to R245fa used in high-temperature heat pumps and organic Rankine cycles. The free convective condensation and pool boiling heat transfer coefficients (HTCs) of these refrigerants on a horizontal smooth tube made of copper with an outer diameter of 19.12 mm are comparatively assessed in this study. For the condensation experiment, the measured HTCs of R1234ze(E) and R1234ze(Z) agree with the theoretical HTC within ±10%. However, the experimental HTC of R1233zd(E) is biased by +25% on average to the theoretical HTC. This suggests the considerable estimation error in R1233zd(E) transport properties. From the pool boiling observations, the role of surface tension on nucleate boiling was identified by the bubble behavior. The experimental boiling HTC closely agrees with the HTC calculated by Ribatski-Jabardo (2003).

Keywords: low GWP, R1234ze(E), R1234ze(Z), R1233zd(E), condensation, pool boiling

NOMENCLATURE

A	heat transfer area	[m^2]
a	thermal diffusivity	[$m^2\ s^{-1}$]
c_p	specific heat	[$J\ kg^{-1}K^{-1}$]
D_b	bubble departure diameter	[m]
D_o	tube outer diameter	[m]
g	gravitational acceleration	[$m\ s^{-2}$]
Ga	Galileo number	[-]
h	enthalpy	[$J\ kg^{-1}$]
h_{LV}	latent heat	[$J\ kg^{-1}$]
Ja	Jakob number	[-]
Ka	Kapitsa number ($= \sigma^3\rho_L/(g\mu_L^4)$)	[-]
L	active heat transfer length	[m]
$\dot{m}$	mass flow rate	[$kg\ s^{-1}$]
M	molar mass	[$kg\ kmol^{-1}$]
Nu	Nusselt number	[-]
P	pressure	[Pa]
Pr	Prandtl number	[-]
p_{red}	reduced pressure ($= P_{sat} / P_{crit}$)	[-]
Q	heat transfer rate	[W]
q_{wall}	heat flux	[$W\ m^{-2}$]
R_a	arithmetic mean surface roughness	[μm]
Ra	Rayleigh number	[-]
Re_f	film Reynolds number ($=4\dot{m}_L/(L\mu_L)$)	[-]
R_p	maximum peak height surface roughness	[μm]
S	standard deviation	[-]
T	temperature	[°C]
T_{film}	film temperature	[°C]
T_{red}	reduced temperature (= (T_{sat}/+273.15) / (T_{tcrit}+273.15))	[-]
V	volumetric flow rate	[$m^3\ s^{-1}$]
X	wavelength	[m]
α	heat transfer coefficient	[$W\ m^{-2}K^{-1}$]
β'	contact angle, 35° in Eq. (11)	[deg]
β	thermal expansion coefficient	[K^{-1}]
$\bar{\varepsilon}$	relative bias	[-]
λ	thermal conductivity	[$W\ m^{-1}K^{-1}$]
μ	viscosity	[Pa·s]
ν	kinetic viscosity	[$m^2\ s^{-1}$]
ρ	density	[$kg\ m^{-3}$]
σ	surface tension	[$N\ m^{-1}$]

Subscripts

cal	calculated value
exp	experimental value

gen heat generation
H_2O cooling / heating water
i inlet
L saturated liquid refrigerant
loss heat leak
o outlet
sat saturation state
V saturated vapor refrigerant
wall tube exterior wall
D_o evaluated at the tube outer diameter

1. Introduction

According to the numbers of atmospheric observations and market analyses (e.g., Velders et al., 2009), the atmospheric burden caused by hydrofluorocarbons (HFCs) has been growing, and this growth is still accelerating owing to their longevity and long application lifecycles. Lunt et al. (2015) reported that the CO_2-equivalent emissions of five HFCs (R134a, R125, R143a, R32, and R152a) increased from 198 Tg-CO_2-eq·yr^{-1} in 2007 to 275 Tg-CO_2-eq·yr^{-1} in 2012. According to an *in-situ* measurement conducted by O'Dohenrty et al. (2014) from 2003 to 2012, the mole fraction in the troposphere was estimated to be 13.4 ppt for R143a and 6.2 ppt for R32 in 2012. Velders et al. (2012) suggested HFC mitigation scenarios with political regulations and concluded that shifting from HFCs to alternative substances with low global warming potential (GWP) will become as important as maintaining energy efficiencies.

The GWPs of hydrofluoro-olefins such as R1233zd(E), R1234ze(E), and the isomer R1234ze(Z), were recently reported to be less than one in IPCC 5AR by Myhre et al. (2013). These substances, especially R1234ze(E), have been intensively studied recently (e.g., Brown et al., 2010). R1234ze(E) is considered a prospective alternative to conventional R134a for car air conditioners, whereas the isomer R1234ze(Z) and R1233zd(E) are anticipated to be the low-GWP alternatives to R245fa used in industrial high-temperature heat pumps, organic Rankine cycles, and so on. Cavallini et al. (2014) evaluated the performance potential of 13 substances including R1234ze(E) and R1234ze(Z) using the second law analysis. Fukuda et al. (2014) suggested that R1234ze(Z) can exhibit higher performance at higher operating temperatures. Nevertheless, the information on their physical properties has not been reported sufficiently for more specific evaluation. The equation of state was proposed for R1234ze(E) and R1234ze(Z) by Akasaka (2011) and Higashi

et al. (2014). For 1233zd(E), the thermodynamic properties and a few transport properties were measured by Hulse et al. (2012). The transport properties of R1234ze(E) were reported by Perkins and Huber (2011), and they are included in REFPROP 9.1 (Lemmon et al., 2013). However, adequately validated transport properties of R1234ze(Z) and R1233zd(E) are not available in the published literature to date, which makes the prediction of heat transfer performance difficult.

Heat transfer performance is a very important factor for determining the irreversible losses in heat exchangers; thus, understanding its characteristics is essential for a complete assessment of the above-mentioned new low-GWP refrigerants. In particular, the data on the free convective condensation and pool boiling are fundamental to the evaluation of the performance of all kinds of heat exchangers used in heat pumps. From the above significance, this study presents the condensation and pool boiling heat transfer coefficients (HTCs) on a horizontal plain tube for the new low-GWP refrigerants. From the experimentally quantified HTCs and visualization results, the HTCs of the new refrigerants are compared to that of the conventional one and the effects of thermophysical properties on HTCs are discussed. To confirm the applicability of the predicting correlations to the new refrigerants, the experimental HTCs are compared to the predicted HTC by the correlations proposed for conventional refrigerants.

2. Experiment

2.1 Experimental setup

Fig. 1 explains the experimental apparatus used in this study. This apparatus is a natural circulation system, which consists of cooling and heating water circuits, and a refrigerant circuit, as illustrated in Fig. 1 (a). The liquid refrigerant condensed on the test tube, installed horizontally in the condensation chamber, and flows down to an evaporation chamber, whereas the refrigerant vapor that evaporated on the test tube flows up to the condensation chamber. The cooling and heating water, which are controlled by the constant temperature bath at a specific temperature and flow rate, are delivered to the condensation and evaporation test tubes. The bulk mean temperatures of cooling and heating water at

the inlet and outlet of the test tubes are measured by platinum resistance thermometers (Pt) in mixing chambers. The volumetric flow rate of water is measured by volumetric flow meters. The refrigerant vapor pressure is measured by an absolute pressure transducer (P) installed near the test tube. Refrigerant temperatures are measured by K-type thermocouples installed circumferentially around the test tubes. The tube wall temperature is obtained using an electric resistance method. As shown in Fig. 1 (b), the test tubes are electrically insulated from the stainless steel chambers and copper piping by plastic sleeves and tubes. Constant direct current is applied to the test tube from just outside the chamber, and the voltage drop over the heat transfer length is measured so that the tube wall temperature can be obtained from the change in electric resistance of the test tube. The plastic-core cylinder is set in the test tube to increase water velocity and improve the water side HTC.

2.2 Experimental conditions

Table 1 lists the experimental conditions. The outer diameter and active heat transfer length of the test tube are 19.12 mm and 400 mm, respectively, for the condensation and evaporation tests. The tested refrigerants are R134a, R1234ze(E), R245fa, R1234ze(Z), and R1233zd(E). The temperature change in the cooling and heating water over the test tube is kept at 3 K. Thus, the temperature distribution of the test tube wall in the flow direction can be suppressed within 2 K over the entire test range. The relative value of the temperature distribution to the subcool/superheat was maximized at the smallest wall subcool/superheat, nevertheless the value was within 13 %. The basic properties of the test refrigerants are summarized in Table 2. The experiments were conducted at saturation temperatures from 20 °C to 60 °C and wall subcool from 0.77 K to 28.81 K for condensation, and saturation temperatures from 10 °C to 60 °C and wall superheat from 1.19 K to 9.17 K.

2.3 Data reduction and measurement uncertainty

The actual heat transfer rate of water Q_{H2O} is calculated as

$$Q_{H_2O} = V_{H_2O}\rho_{H_2O}\left|h_{H_2O,o} - h_{H_2O,i}\right| - Q_{loss}, \quad (1)$$

where V_{H2O}, ρ_{H2O}, and h_{H2O} are the volumetric flow rate, density, and specific enthalpy of the cooling/heating water, respectively. The water density is evaluated at a temperature measured in a mixing chamber placed at the outlet of the test tube, as shown in Fig. 1 (a). The inlet and outlet specific enthalpies, $h_{H2O,i}$ and $h_{H2O,o}$, are evaluated at the inlet and outlet water temperatures, respectively. Q_{loss} is the heat loss from the cooling/heating water to ambient air. This heat loss is preliminarily measured and proportionally correlated with the temperature difference between the cooling/heating water and ambient air. For instance, when the temperature difference is 10 K, the heat loss is approximately 6.5 W. This corresponds to 1.3% of the actual heat transfer rate. The heat flux based on the outer surface area of the test tube, q_{wall}, is calculated as,

$$q_{wall} = \frac{Q_{H_2O}}{\pi D_o L}, \quad (2)$$

where D_o and L are the outer diameter and active heat transfer length of the test tube, respectively. The HTC, α, based on the outer surface is defined as

$$\alpha = \frac{q_{wall}}{\left|T_{sat} - T_{wall}\right|}, \quad (3)$$

where T_{wall} is the average wall temperature obtained by means of the electric resistance method. From the calibration results, it was confirmed that the wall temperature can be determined with an uncertainty of ±0.078 K by the electric resistance method. T_{sat} is the saturation temperature calculated from the measured pressure with REFPROP 9.1 (Lemmon et al., 2013), assuming a thermal equilibrium state.

Table 3 lists the instruments, measurement methods, and measurement uncertainty. The 95% coverage of uncertainties propagated with several variables are obtained by means of the square-root rule (Taylor, 1982), assuming independent variables and random errors. The calculation procedure is specified in Appendix A. The measurement uncertainty in the heat loss, Q_{loss}, is unknown; therefore, 100% of the heat loss is taken into account in the uncertainty.

2.4 Refrigerant purity

The test refrigerants provided by the manufacturer were purified in the experimental apparatus before starting the experiment. Non-condensable gases are mostly contained in the vapor phase. However, even minute amounts of these gases severely diminish the free convective condensation heat transfer (Minkowycz and Sparrow, 1966) at smaller wall subcools. The condensation chamber filled with refrigerant vapor containing non-condensable gases was separated from the other volumes by closing valves, and these gases were carefully evacuated using a vacuum pump. Then, by opening the valves, the evaporated refrigerant vapor and non-condensable gasses dissolved in liquid vapor were drawn into the condensation chamber. By repeating this procedure, the non-condensable gasses were eliminated from the experimental apparatus.

Fig. 2 shows the change in condensation HTC during the purification procedure. The symbols show the experimental HTC of R1234ze(Z) as a function of wall subcool at a saturation temperature of 20 °C. The solid line shows the theoretical HTC of R1234ze(Z) alone (Nusselt, 1916). As the procedure is repeated, the HTC gradually increases up to the theoretical HTC. By the 6th repetition, the experimental HTC reached the theoretical HTC, which suggests an absence or negligible amount of non-condensable gasses. The 7th data series was recorded after several experimental runs. The repeatability of the experimental method is validated by the highly overlapped 6th and 7th data series. R1233zd(E) and R245fa were also purified using the abovementioned procedure.

3. Condensation Experiment

3.1 Condensation HTC of R1234ze(E), R1234ze(Z), and R1233zd(E)

Figs. 3(a) to 3(c) plot the condensation HTC on the horizontal tube for R1234ze(E), R1234ze(Z), and R1233zd(E) at saturation temperatures of 20 °C, 40 °C, and 60 °C, respectively. The symbols show the experimentally determined HTC,

with vertical and horizontal bars indicating the measurement uncertainties in HTC and wall subcool, respectively. Meanwhile, the lines show the theoretical HTC calculated by the Nusselt theory (Nusselt, 1916):

$$\alpha = \frac{\lambda_{\mathrm{L}}}{D_{\mathrm{o}}} Nu = 0.728 \frac{\lambda_{\mathrm{L}}}{D_{\mathrm{o}}} \left(\frac{GaPr_{\mathrm{L}}}{Ja} \right)^{0.25} = 0.728 \left[\frac{g}{D_{\mathrm{o}} \left(T_{\mathrm{sat}} - T_{\mathrm{wall}} \right)} \right]^{0.25} \left\{ \lambda_{\mathrm{L}}^{0.75} \cdot \left[\rho_{\mathrm{L}} \left(\rho_{\mathrm{L}} - \rho_{\mathrm{V}} \right) \right]^{0.25} \cdot h_{\mathrm{LV}}^{0.25} \cdot \mu_{\mathrm{L}}^{-0.25} \right\},$$
$$Ga = \frac{g D_{\mathrm{o}}^3}{\nu_{\mathrm{L}}^2} \left(\frac{\rho_{\mathrm{L}} - \rho_{\mathrm{V}}}{\rho_{\mathrm{L}}} \right), \quad Pr_{\mathrm{L}} = \frac{\mu_{\mathrm{L}} c_{\mathrm{pL}}}{\lambda_{\mathrm{L}}}, \quad Ja = \frac{c_{\mathrm{pL}} \left(T_{\mathrm{sat}} - T_{\mathrm{wall}} \right)}{h_{\mathrm{LV}}} \tag{4}$$

where Nu, Ga, Pr_{L}, and Ja are the Nusselt number, Galileo number, Prandtl number, and Jakob number, respectively, and g, ν, ρ, μ, c_{p}, λ, and h_{LV} are the gravitational acceleration, kinematic viscosity, density, viscosity, specific heat capacity, thermal conductivity, and latent heat, respectively. The latent heat h_{LV} is evaluated at a saturation temperature, whereas the other properties are evaluated at a film temperature, $T_{\mathrm{film}} = \left(T_{\mathrm{sat}} + T_{\mathrm{wall}} \right) / 2$. The experimental HTCs show good agreement with the Nusselt theory for R1234ze(E) and R1234ze(Z). Because the theory was derived under simple conditions, omitting the sensible heat transfer (e.g., heat with a degree of subcool and superheat) and convective effect, the theoretical HTC could indicate slightly lower than the actual values. For R1233zd(E), however, the experimental HTC deviates considerably from the theoretical values. Although the sensitivity of wall subcool in the experimental HTC agrees qualitatively with the theory, the experimental HTC is approximately 20% higher than the theoretical values. This is beyond the measurement uncertainty.

Fig. 4 compares the experimentally obtained Nusselt number, Nu, against $(Ga \cdot Pr_{\mathrm{L}} / Ja)$ expressed in the Nusselt theory (Eq. (4)) for R134a, R1234ze(E), R245fa, R1234ze(Z), and R1233zd(E). The solid line represents the Nusselt theory. As shown in Fig. 4, the Nu of R1233ze(Z) obviously differs from the other experimental Nu and theoretical Nu. To quantify the degree of deviation in the experimental Nu from the theoretical Nu, the average bias, $\bar{\varepsilon}$, and two-standard deviation, $2S$, are calculated as follows:

$$\bar{\varepsilon} = \frac{1}{N} \sum_{j=1}^{N} \varepsilon_j = \frac{1}{N} \sum_{j=1}^{N} \left(\frac{Nu_{\mathrm{exp},j} - Nu_{\mathrm{cal},j}}{Nu_{\mathrm{cal},j}} \right) \tag{5}$$

$$2S = 2\sqrt{\frac{1}{N-1}\sum_{j=1}^{N}\left(\varepsilon_j - \bar{\varepsilon}\right)^2}\ , \tag{6}$$

where N is number of the data. These values, $\bar{\varepsilon}$ and $2S$, are denoted in Fig. 4. The experimental Nu of R1234ze(E) and R1234ze(Z) distributes with a bias of +6% in a two-standard deviation of ±10%. This confirms that the calculated thermophysical properties of R1234ze(E) and R1234ze(Z) using REFPROP 9.1 are adequately accurate for predicting the condensation HTC. On the other hand, the experimental Nu of R1233zd(E) is biased by +25.4%, on average, relative to the theoretical Nu. Because of a lack of measured data on R1233zd(E) physical properties, most of the properties are estimated internally by the REFPROP 9.1 program. Hence, at present, REFPROP 9.1 cannot guarantee high accuracy in the estimated properties. Perhaps the estimation error, especially in the transport properties such as thermal conductivity, caused this considerably large bias for R1233zd(E).

3.2 Comparison between conventional and alternative refrigerants

Fig. 5 compares the condensation HTCs between conventional refrigerant and the candidate for the alternative refrigerant. In Fig. 5 (a), the HTCs of R134a and R1234ze(E) are compared at a saturation temperature of 40 °C. In Fig. 5 (b), the HTCs of R245fa, R1234ze(Z), and R1233zd(E) are compared at a saturation temperature of 60 °C. The HTC of R1234ze(E) is approximately 8% lower than that of R134a. This can be explained by the 8% lower liquid thermal conductivity and 5% smaller latent heat of R1234ze(E), relative to those of R134a. The HTC of R1234ze(Z) is approximately 10% higher than that of R245fa. This can be explained by the 11% lower liquid viscosity and 8% larger latent heat of R1234ze(Z), relative to those of R245fa. The HTC of R1233zd(E) is comparable to that of R245fa. This cannot be explained with the currently available property data. Table 4 analyses the contribution of thermophysical properties in the HTC at a saturation temperature of 40 °C and wall subcool of 10 K for R134a and R1234ze(E), and at a saturation temperature of 60 °C and a wall subcool of 10K for R245fa, R1234ze(E), and R1233zd(E). These are estimated along the Nusselt equation expressed by Eq. (4). According to the Nusselt theory, the HTC is proportional to

$\lambda_L^{0.75}$, $\left[\rho_L\left(\rho_L-\rho_V\right)\right]^{0.25}$, $h_{LV}^{0.25}$, and $\mu_L^{-0.25}$. As listed in Table 4, the thermal conductivity strongly distinguishes the HTC of R1234ze(E) from R134a. Between R1234ze(Z) and R245fa, the effects of thermal conductivity, latent heat, and especially viscosity compensate the effects of density. As a consequence, the HTC R1234ze(Z) is increased by 4% from that of R245fa. The calculated relativity of HTCs identifies the experimentally obtained relativity in HTC between R134a and R1234ze(E), R245fa, and R1234ze(Z), as shown in Figs. 5(a) and 5(b). However, this shows inconsistency for R1233zd(E). According to the calculation results using the estimated properties, the HTC of R1233zd(E) is expected to be 16% lower than that of R245fa, mainly due to the lower liquid thermal conductivity. On the other hand, the experimental results of R1233zd(E) exhibit an HTC that is almost comparable to that of R245fa. To scrutinize this inconsistency in HTC relativity, more accurate transport properties based on measurements would be necessary for R1233zd(E).

3.3 Condensate behavior

Figs. 6 (a) to 6 (i) are photographs showing the condensate flow modes of R1234ze(E), R1234ze(Z), and R1233zd(E). The condensate flow mode is droplet for most of the experimental conditions. To categorize the condensate flow modes, the following K-factor, K, and film Reynolds number, Re_f, are introduced by Yung et al. (1980):

$$K=\frac{\dot{m}_L}{L}\frac{\left(g/\rho_L\right)^{0.25}}{2\sigma^{0.75}},\quad Re_f=\frac{4\left(\dot{m}_L/L\right)}{\mu_L}=\frac{4Q_{H_2O}}{\mu_L h_{LV}L}. \tag{7}$$

where $\dot{m}_L$ and σ are the total mass flow rate and surface tension of the condensate, respectively. According to the report by Yung et al., the flow mode shifts from droplet to column and from column to sheet with increasing K and Re_f. As shown in Figs. 6 (c), (f), and (i), the droplet-column modes are observed in the high-film Reynolds number, Re_f, region. According to Yung et al. (1980), the column mode can be seen for K-factors above 0.061. As shown in Figs. 6 (c) and (i), some liquid columns can be observed for K-factors of 0.068 and 0.061. At a K-factor of 0.069, shown in Fig. 6 (f), it appears that the shift to the column mode is somewhat more advanced. Hence, the observed condensate of the tested refrigerant meets this criterion in general.

The spacing of the falling droplet arrays and columns, denoted as *X* in Fig. 6 (i), is typically called a wavelength. Fig. 7 compares the wavelengths of the tested refrigerants at a saturation temperature of 40 °C. The symbols are the average of measured wavelengths at each of the six positions in the 10 photographs taken at a given condition. The wavelength of R1234ze(E) is evidently shorter than the others. The other three refrigerants exhibit similar wavelengths. A theoretical model to predict the wavelength using Taylor instability was proposed by Bellman and Pennington (1953). Later, an empirical correlation was proposed by Armbruster and Mitrovic (1998).

$$\begin{cases} X = \left(2\pi\sqrt{2}\right) \Big/ \sqrt{\dfrac{g\left(\rho_{\mathrm{L}}-\rho_{\mathrm{V}}\right)}{\sigma}\left[1+\dfrac{\left(Re_{\mathrm{f}}/4\right)^{0.8}}{Ka^{0.2}}\right]+\dfrac{2}{D_{\mathrm{o}}{}^{2}}} \\ Ka = \sigma^{3}\cdot\rho_{\mathrm{L}} \Big/ \left(g\mu_{\mathrm{L}}{}^{4}\right) \end{cases} \tag{8}$$

The correction factor of $\left[\left(Re_{\mathrm{f}}/4\right)^{0.8}\Big/Ka^{0.2}\right]$ was omitted here as zero. This simplification was justified by the larger measurement uncertainty for the comparison with the measured wavelengths. Despite the above, a correlation was proposed for water film evaporation, and the predicted values agreed with the measured wavelengths (within the uncertainty).

The facts found from the visualization results support the accuracy of properties influencing condensate behavior. Most likely, the liquid and vapor densities, surface tension, and liquid viscosity of R1233zd(E) are not the cause of the inconsistency in its condensation heat transfer.

4. Pool Boiling Experiment

4.1 Hysteresis of nucleate boiling inception: a departure from single-phase natural convection

Fig. 8 shows a series of typical experimental data at a saturation temperature of 30 °C for R245fa. The filled and unfilled symbols represent the data series for increasing and decreasing heat flux, respectively. The lines represent the HTC calculated by the correlations proposed for single-phase natural convection on cylinders, recommended by Boetcher

(2014).

Wamsler (1911):
$$\begin{cases} Nu_{D_o} = \dfrac{\alpha D_o}{\lambda_l} = 0.48 Ra_{D_o}{}^{0.25}, \\ Ra_{D_o} = g\beta\left(T_{wall} - T_{sat}\right) D_o{}^3 / \nu^2 \end{cases} \tag{9}$$

Fujii et al. (1979):
$$\begin{cases} \dfrac{2}{Nu_{D_o}} = \ln\left[1 + \dfrac{4.065}{C_1 Ra_{D_o}{}^m}\right], \\ C_1 = 0.671\left[1 + \left(\dfrac{0.496}{Pr_L}\right)^{9/16}\right]^{-4/9}, \quad m = \dfrac{1}{4} + \dfrac{1}{10 + 4Ra_{D_o}{}^{1/8}} \end{cases} \tag{10}$$

and the correlation proposed for the nucleate boiling of refrigerants:

Stephan-Abdelsalam (1980):
$$\begin{cases} Nu = \dfrac{\alpha D_b}{\lambda_L} = 207\left[\dfrac{q_{wall} D_b}{\lambda_L\left(T_{sat} + 273.15\right)}\right]^{0.745}\left(\dfrac{\rho_V}{\rho_L}\right)^{0.581} Pr_L{}^{0.533}, \\ D_b = 0.0146\beta'\sqrt{\dfrac{2\sigma}{g\left(\rho_L - \rho_V\right)}}, \quad \beta' = 35^{\circ} \end{cases} \tag{11}$$

For the operation of increasing heat flux, the first two data points exhibit the single-phase natural convection HTC. Data points (a) and (b) exhibit decreasing wall superheat due to partially incipient nucleate boiling. Figs. 9 (a) to (d) are the visualization results for the data points from (a) to (d) denoted in Fig. 8. Figs. 9 (a) and (b) identify the inception of partial nucleate boiling. Then, at heat fluxes beyond 20 kWm^{-2}, as shown by data point (c) in Fig. 8 and the photograph in Fig. 9 (c), the nucleate boiling is fully developed, and the experimental HTC agrees with the Stephan-Abdelsalam correlation (1980). However, for the operation of decreasing heat flux, the HTC stays along the nucleate boiling correlation line at heat fluxes down to 1.5 kWm^{-2}. As shown in Fig. 9 (d), frequent bubble departure is observed at a heat flux of 12 kWm^{-2}. The two different boiling curves in Fig. 8 indicate that more wall superheat is encountered by the operation of increasing heat flux for nucleate boiling inception (BarCohen, 1992; Shi et al., 1993). According to early investigations (e.g., Lian and Yang, 1998), this overshoot in wall superheat can be intensified with high wetting combinations of fluid and surface. The test tube was degreased and well-cleansed with ethanol immediately before the installation. With this procedure, this hysteresis was evident for all of the test refrigerants. To simplify the heat transfer assessment, hereafter, only the data for fully developed nucleate boiling are selected with visualization results.

4.2 Comparative assessment of fully developed nucleate boiling HTC for low-GWP refrigerants

Figs. 10 (a), (b), and (c) compare the experimental HTCs at saturation temperatures of 10 °C, 40 °C, and 60 °C, respectively, for R134a, R1234ze(E), R245fa, R1234ze(Z), and R1233zd(E). From the observation results, the HTC data of either natural convection or partial boiling are eliminated from the nucleate boiling data plotted in Fig. 10. The horizontal and vertical bars appended to the symbols indicate the uncertainty ranges in heat flux and HTC. The lines indicate the HTCs calculated by the correlation

Ribatski and Jabardo (2003): $$\begin{cases} \alpha = 100 \times {q_{\text{wall}}}^{n} {p_{\text{red}}}^{0.45} \left[-\log p_{\text{red}} \right]^{-0.8} {R_{\text{a}}}^{0.2} M^{-0.5}, \\ n = 0.9 - 0.3 {p_{\text{red}}}^{0.2} \end{cases} \quad (12)$$

where p_{red} and M are the reduced pressure and molar mass in kg kmol^{-1} of the refrigerants. R_{a} is the arithmetic mean surface roughness of the test tube in μm. This correlation uses the reduced parameter and does not need any transport parameters.

Comparing HTCs at a given saturation temperature and heat flux, the HTCs of R134a and R1234ze(E) are obviously higher than those of the other refrigerants. The HTC of R1234ze(E) is slightly lower than that of R134a. The HTCs of R1234ze(Z) and R1233zd(E) are slightly higher and are lower than that of R245fa, respectively. These differences are attributed to the thermophysical properties of the refrigerants. Because of the lower critical pressures of R134a and R1234ze(E) relative to the other three refrigerants, these two refrigerants are operated at higher reduced pressures and at saturation temperatures of 10 °C and 40 °C. Thus, for instance, the smaller surface tension and density ratio of liquid to vapor can be predicted from the principle of corresponding states. In numerous early studies, it was found that decreasing these properties enhances the nucleate boiling heat transfer at higher reduced pressures for most of the refrigerants, even though some other property changes such as the Pr_{L} change compensate for this. Specifically, surface tension is an important factor in determining the bubble departure diameter (i.e., equilibrium break-off diameter) D_{b} and bubble behavior. As shown in Eq. (11), Fritz (1935) introduced a model $\{2\sigma/[g(\rho_{\text{L}}\text{-}\rho_{\text{V}})]\}^{1/2}$ from Rayleigh's theory in which the diameter D_{b} is dictated by the balance between buoyancy force and surface tension force under thermodynamic equilibrium. This model provides a smaller bubble diameter D_{b} at higher pressures. Later, a relation was drawn up

between the bubble departure frequency f_b and diameter $f_b D_b$ = const. (e.g., Malenkov, 1970). From this relation, it is clear that bubble departure is more frequent for small bubbles. Additionally, a higher nucleation site density (or larger number of active nucleation cavities) is expected because smaller bubble embryos can grow under smaller surface tension. The surface tensions of the tested refrigerants were measured by Tanaka and Higashi (2013) and Kondou et al. (2015). According to their work, at a given temperature, the surface temperatures of R134a and R1234ze(E) are evidently smaller than those of the other tested refrigerants. The order of surface tension is exactly the inverse of that of the HTC. This supports the role of surface tension in nucleate boiling mentioned above.

Figs. 11 (a) to (e) are photographs of bubble formation on the tube surface for tested refrigerants at a saturation temperature of 20 °C and a heat flux of 20 kWm^{-2}. The reduced pressures p_{red} and the experimental HTC α are denoted in the captions. The diameter and number of bubbles are apparently smaller and greater, respectively, for R134a and R1234ze(E) than those for the other three refrigerants. The experimentally quantified HTCs are 5.45 $kWm^{-2}K^{-1}$ and 4.21 $kWm^{-2}K^{-1}$ for R134a and R1234ze(E), respectively, whereas the HTCs of R245fa, R1234ze(Z), and R1233ze(E) are 2.00 $kWm^{-2}K^{-1}$, 2.46 $kWm^{-2}K^{-1}$, and 1.66 $kWm^{-2}K^{-1}$, respectively. Comparing Figs. 11 (f) to (d), the nucleation site density of R1234ze(Z) is significantly increased as the saturation temperature increases.

Fig. 12 plots the nucleation site density in cm^{-2} and the bubble departure diameter estimated by Eq. (11) against the reduced pressure. The nucleation site density is quantified by video images recorded during 5 sec by a high-speed microscope camera at saturation temperatures of 20 °C and 40 °C and a heat flux of 7 kWm^{-2} for R245fa, R1234zd(Z), and R1233zd(E). Fig. 13 explains the procedure to measure the nucleation site density. The number of sites, where the bubble growth was observed even once in 5 sec, in a surface area of 688 mm^2 at the center of test tube was counted frame by frame. While the multiple counting was avoided by marking. As plotted in Fig.12, the nucleation site density significantly increases with increasing reduced pressure. This means the increase in the number of active nucleation

cavities on the surface of the test tube. Conversely, the estimated bubble departure diameter, D_b, decreases. Meanwhile, the HTC increases, as indicated in Fig. 11. These visualization results thereby identify the bubble behavior and the abovementioned mechanism of nucleate boiling enhancement. The higher performance of nucleate boiling heat transfer can be expected for systems operated at higher temperatures (i.e., at higher reduced pressures) for R245fa, R1234ze(Z), and R1233zd(E).

4.3 Comparison for correlations with "estimated transport properties"

Recently, thermodynamic property data and equations of state (Akasaka, 2011; Hulse et al., 2012; Higashi et al., 2014; Mondejar et al., 2015) and surface tension data (Tanaka and Higashi, 2013; Kondou et al., 2015) were reported for the low-GWP refrigerants tested here. Transport properties were reported by Perkins and Huber (2011) and Miyara et al. (2011) for R1234ze(E). Nevertheless, the data are still insufficient or unavailable for R1234ze(Z) and R1233zd(E). Therefore, REFPROP 9.1 (Lemmon et al., 2013) claims an estimation uncertainty of 20% for these transport properties. The HTC prediction is highly difficult with physics-based correlations. In addition to the above correlations, including Stephan-Abdelsalam (1980) and Ribatski-Jabardo (2003), for comparison, the following two correlations were selected:

Jung et al. (2003):
$$\begin{cases} \alpha = 10\dfrac{\lambda_L}{D_b}\left[\dfrac{q_{wall}D_b}{\lambda_L\left(T_{sat}+273.15\right)}\right]^{C_1} p_{red}\left(1-T_{red}\right)^{-1.4}\left(\dfrac{v_L}{a_L}\right)^{-0.25}, \\ C_1 = 0.855\left(\dfrac{\rho_V}{\rho_L}\right)^{0.309} p_{red}{}^{-0.437} \end{cases} \tag{13}$$

Gorenflo et al. (2010):
$$\begin{cases} \alpha = 3580\left[\left(\dfrac{dP}{dT}\right)_{sat,\ at\ p_{red}=0.1}\Big/\sigma\right]^{0.6}\left(\dfrac{q_{wall}}{20000}\right)^{nq}\left(\dfrac{R_a}{0.4}\right)^{2/15} F_{p_{red}}, \\ nq = 0.95-0.3p_{red}{}^{0.3},\ \ F_{p_{red}} = 0.7p_{red}{}^{0.2}+4p_{red}+1.4p_{red}/\left(1-p_{red}\right) \end{cases} \tag{14}$$

where $(dP/dT)_{sat,\ at\ pred=0.1}$ in Eq. (14) is the slope of the saturation vapor pressure curve at a reduced pressure of 0.1.

Table 5 lists the relative bias, $\overline{\varepsilon}$, and standard deviation, S, of the calculated HTC, α_{cal}, from the experimental HTC, α_{exp}, for each correlation. Among the selected correlations, that of Ribatski-Jabardo (2003) showed the best

agreement with the experimental data. This correlation uses no specific property data but only reduced pressure. Hence, only the critical pressure is necessary. This simple method successfully evaluates HTC relativity with very limited information, whereas the correlations that require transport properties such as λ_L and a_L can result in different HTC relativity even among R245fa, R1234ze(Z), and R1233zd(E) with the currently available data. Once accurate transport property data are reported, the prediction results on nucleate boiling HTC should be improved.

5. Conclusions

Free convective condensation and pool boiling HTC on horizontal plain tubes have been experimentally assessed for the low GWP refrigerants R1234ze(E), R1234ze(Z), and R1233zd(E).

As the elimination of noncondensable gases proceeded, the free convective condensation HTC increased up to the HTC of Nusselt theory. The HTC of R1234ze(E) is slightly lower than that of R134a. The HTCs of R1234ze(Z) is somewhat higher than that of R245fa; while the HTC of R1233zd(E) is comparable to R245fa. The experimental condensation HTC agrees with Nusselt theory, except for R1233zd(E). Only the data of R1233zd(E) deviates beyond the measurement uncertainty from the theoretical HTC calculated with the estimated transport properties. By the observation of falling condensate, the shift from droplet to column mode was confirmed at a K factor of nearly 0.061, which meets the criterion of Yung et al. (1980). The wavelength was identical to the prediction of Armbruster and Mitrovic (1998). The observation results suggest that the calculated liquid and vapour densities and surface tensions are adequately accurate.

From the viewpoint of nucleate boiling heat transfer on horizontal tubes, low GWP refrigerants R1234ze(E), R1234ze(Z), and R1233zd(E) are assessed at saturation temperatures from 10 °C to 60 °C and heat fluxes from 0.7 kWm^{-2} to 80 kWm^{-2}. The pool boiling HTC of R1234ze(E) is slightly lower than that of R134a, whereas the HTCs of the other three refrigerants are significantly lower. The HTC of R1234ze(Z) and R1233zd(E) is slightly higher and is lower than that of R245fa, respectively. This HTC relativity can be explained with vitalized bubble size, nucleation site density,

and surface tension data. Among the selected correlations, that of Ribatski-Jabardo (2003) using only reduced pressure (i.e., critical pressure) showed the best agreement with the experimental data. This simple method successfully evaluates HTC relativity with very limited information. For the prediction methods based on physical properties, accurate transport property data are needed.

Acknowledgements

The present study is sponsored by the project on the "Development of High Efficiency and Non-Freon Air Conditioning Systems" of the New Energy and Industrial Technology Development Organization (NEDO) Japan. The tested R245fa and R1233zd(E) were kindly supplied by Central Glass Co., Ltd., Japan.

Appendix A. Uncertainty analysis

For a system involving independent and random errors, the error propagation of 95% coverage by the several variables can be given by a square-root rule (Taylor, 1982). With this method, the uncertainty in the experimentally quantified values in this study is estimated.

The heat transfer area is given as,

$$A = D_o \pi \times L \tag{A.1}$$

Thus the uncertainty in the heat transfer area U_A is calculated from the following equations.

$$U_A = \sqrt{\left(L\pi \cdot U_{D_o}\right)^2 + \left(D_o \pi \cdot U_L\right)^2} \tag{A.2}$$

where U_{D_o} and U_L are the uncertainty in the tube outer diameter and the active heat transfer length, listed in Table 3. While, the uncertainty in actual heat transfer rate obtained from Eq. (1) is estimated as,

$$U_{Q_{H2O}} = \sqrt{\left(V_{H_2O}\rho_{H_2O} \cdot U_{\Delta h_{H_2O}}\right)^2 + \left(\left|h_{H_2O,o} - h_{H_2O,i}\right| \rho_{H_2O} \cdot U_{V_{H_2O}}\right)^2 + U_{Q_{loss}}{}^2} \tag{A.3}$$

The uncertainty in enthalpy change of heat cooling/heating water, $U_{\Delta h_{H_2O}}$, is given as,

$$U_{\Delta h_{\mathrm{H_2O}}} = U_{h_{\mathrm{H2O,o}}} + U_{h_{\mathrm{H2O,i}}} \tag{A.4}$$

Each uncertainty $U_{h_{\mathrm{H2O,o}}}$ and $U_{h_{\mathrm{H2O,i}}}$ is determined by the uncertainty in water temperature measured by the Pt resistance thermometer ±0.05 K. The uncertainty in volumetric flow rate of the water, $U_{V_{\mathrm{H_2O}}}$, depends on the reading value, $V_{\mathrm{H_2O}}$.

$$U_{V_{\mathrm{H_2O}}} = V_{\mathrm{H_2O}} \times 0.005 \tag{A.5}$$

The uncertainty in heat loss, $U_{Q_{\mathrm{loss}}}$, is assumed same as the heat loss preliminarily measured. This uncertainty is correlated to the temperature difference between cooling/heating water and ambient air. Therefore, the uncertainty in heat flux is,

$$U_{q_{\mathrm{wall}}} = \sqrt{\left(\frac{1}{A} U_{Q_{\mathrm{H2O}}}\right)^2 + \left(\frac{Q_{\mathrm{H2O}}}{A^2} U_A\right)^2} \tag{A.6}$$

The degree of wall subcool and superheat is,

$$\Delta T_{\mathrm{wall}} = \left| T_{\mathrm{sat}} - T_{\mathrm{wall}} \right| \tag{A.7}$$

The saturation temperature T_{sat} is a function of pressure. Thus, the uncertainty in saturation temperature $U_{T_{\mathrm{sat}}}$ is determined from the measured pressure P, the uncertainty U_P, and the calculation uncertainty from REFRPOP. The uncertainty in saturation temperature caused by the uncertainty of pressure measurement is approximately 0.05 K. On the other hand, the calculation uncertainty in saturation temperature from the equation of state in REFPROP is within 0.006 K (Akasaka et al., 2014; Mondéjar et al., 2015). Thus the total uncertainly in the saturation temperature is estimated to be 0.056 K. The uncertainty in tube wall temperature $U_{T_{\mathrm{wall}}}$ is obtained from the calibration results as listed in Table 3. From these, the uncertainty in degree of wall subcool and superheat is,

$$U_{\Delta T_{\mathrm{wall}}} = \sqrt{U_{T_{\mathrm{sat}}}{}^2 + U_{T_{\mathrm{wall}}}{}^2} \tag{A.8}$$

The uncertainty in heat transfer coefficient is estimated from the above uncertainties $U_{q_{\mathrm{wall}}}$ and $U_{\Delta T_{\mathrm{wall}}}$.

$$U_\alpha == \sqrt{\left(\frac{1}{\Delta T_{\mathrm{wall}}} U_{q_{\mathrm{wall}}}\right)^2 + \left(\frac{q_{\mathrm{wall}}}{\Delta T_{\mathrm{wall}}{}^2} U_{\Delta T_{\mathrm{wall}}}\right)^2}$$

Depending on the experimental conditions, the uncertainties range widely. Therefore, the uncertainty in heat transfer coefficient, heat flux, and wall subcool are shown with bars appended to the symbols in Figs. 3, 5 and 9 for each measurement point.

REFERENCES

Akasaka, R., 2011. New Fundamental Equations of State with a Common Functional Form for 2,3,3,3-Tetra fluoropropene (R-1234yf) and Trans-1,3,3,3-Tetrafluoropropene (R-1234ze(E)), *Int. J. Thermophysics*, 32 (6) 1125-1147.

Akasaka, R., Higashi, Y, Miyara, A, Koyama, S, 2014. A fundamental equation of state for cis-1,3,3,3-tetrafluoropropene (R-1234ze(Z)), *Int. J. Refrig.*, 44, 168-176.

Armbruster, R., Mitrovic, J., 1998. Evaporative cooling of a falling water film on horizontal tubes. *Exp. Therm. Fluid Sci*., 18, 183-194.

ASHRAE STANDARD, 2011. ANSI/ASHRAE Standard 34-2010, Designation and safety classification of refrigerants.

ASHRAE STANDARD, 2015. Addenda Supplement to ANSI/ASHRAE Standard 34-2013, Designation and safety classification of refrigerants.

BarCohen, A., 1992. Hysteresis phenomena at the onset nucleate boiling. *Proc. Engineering Foundation Conf. Pool and Engineering Flow Boiling*. Santa Barbara, California, 1-14.

Bellman, R., Pennington, R.H., 1953. Effects of surface tension and viscosity on Taylor instability, Santa Monica, CA: RAND Corporation, http://www.rand.org/pubs/papers/P403.

Boetcher, S.K.S, 2014. Natural Convection from Circular Cylinders, *Springer Briefs in Applied Science and Technology, Thermal Engineering and Applied Science*, 3-22.

Brown, J.S., Zilio, C., Cavallini, A., 2010. Thermodynamic properties of eight fluorinated olefins. *Int. J. Refrig*., 33, 235-241.

Cavallini, A., Zilio, C., Brown, J.S., 2014. Sustainability with prospective refrigerants. Energy Research, 38, 285-298.

Fritz, W., 1935. Berechnung des Maximal Volumens von Dampfblasen (Maximum volume of vapor bubbles). *Physikalishe Zeitschrift*, 36, 379-384.

Fujii, T., Fujii, M., Matunaga, R., 1979. A numerical analysis of laminar free convection around an isothermal horizontal circular cylinder, *Numerical Heat Transfer*, 2 (3) 329-344.

Fukuda, S., Kondou, C., Takata, N., Koyama, S., 2014. Low GWP refrigerants R1234ze(E) and R1234ze(Z) for high temperature heat pumps. *Int. J. Refrig*. 40, 161-173.

Gorenflo, D., Baumhögger, E., Windmann, T., Herres, G., 2010. Nucleate pool boiling, film boiling and single-phase free convection at pressures up to the critical state. Part I: Integral heat transfer for horizontal copper cylinders. *Int. J. Refrig.*, 33, 1229-1250.

Higashi, Y., Hayasaka, S., Shirai, C., Akasaka, R., 2015. Measurements of PρT properties, vapor pressures, saturated densities, and critical parameters for R 1234ze(Z) and R 245fa. *Int. J. Refrig*., 52, 100-108.

Hulse, R.J., Basu, R.S., Singh, R.R., Thomas, R.H.P., 2012. Physical Properties of HCFO-1233zd(E). *J. Chem. Eng. Data*, 57, 3581-3586.

Jung, D., Kim, Y., Ko, Y., Song, K., 2003. Nucleate boiling heat transfer coefficients of pure halogenated refrigerants. *Int. J. Refrig*., 26, 240-248.

Kondou, C., Nagata, R., Nii, N., Koyama, S., Higashi, Y., 2015. Surface tension of low GWP refrigerants R1243zf, R1234ze(Z), and R1233zd(E). *Int. J. Refrig.*, 53, 80–89.

Koyama, S., Higashi, T., Miyara, A. Akasaka, R., 2013. JSRAE Risk Assessment of Mildly Flammable Refrigerants-2012 Progress Report, 29-34.

Lemmon, E.W., Huber, M.L., McLinden, M.O., 2013. Reference Fluid Thermodynamic and Transport Properties - REFPROP Ver. 9.1. National Institute of Standards and Technology, Boulder, CO, USA.

Lian, H.S., Yang, W.J, 1998. Nucleate pool boiling heat transfer in a highly wetting liquid on micro-graphite-fiber composition surface. *Int. J. Heat Mass Transf.*, 41 (13) 1993-2001.

Lunt, M.F., Rigby, M., Ganesan, A.L., Manning, A.J., Prinn, R.G., O'Doherty, S., Mühle, J., Harth, C.M., Salameh, P.K., Arnold, T., Weiss, R.F., Saito, T., Yokouchi, Y., Krummel, P.B., Steele, L.P., Fraser, P.J., Li, S., Park, S., Reimann, S., Vollmer, M.K., Lunder, C., Hermansen, O., Schmidbauer, N., Maione, M., Arduini, J., Young, D., Simmonds, P.G., 2015. Reconciling reported and unreported HFC emissions with atmospheric observations. *Proc. Natl. Acad. Sci.* 201420247.

Malenkov, I.G., 1970. Detachment frequency as a function of size for vapor bubbles, Heat Phusics Institute, Siberian Division, Academy of Sciences of the USSR Novsibirsk. Translated from *Inzhenerno-Fizicheskii Zhurnal*, vol. 20, no. 6, 988-994.

Minkowycz, W.J., Sparrow, E.M., 1966. Condensation heat transfer in the presence of noncondensables, interfacial resistance, superheating, variable properties, and diffusion. *Int. J. Heat Mass Transf.*, 9, 1125-1144.

Miyara, A., Fukuda, R., Tsubaki, K., 2011. Thermal conductivity of saturated liquid of R1234ze(E)+R32 and R1234yf+R32 mixtures. Trans. JSRAE, 28 (4) 435-443.

Mondéjar, M.E., McLinden, M.O., Lemmon, E.W., 2015. Thermodynamic Properties of trans -1-Chloro-3,3,3-trifluoropropene (R1233zd(E)): Vapor Pressure, (p, ρ, T) Behavior, and Speed of Sound Measurements, and Equation of State. *J. Chem. Eng. Data*, 60, 2477-2489.

Myhre, G., Shindell, D., Bréon, F.M., Collins, W., Fuglestvedt, J., Huang, J., Koch, D., Lamarque, J.F., Lee, D., Mendoza, B., Nakajima, T., Robock, A., Stephens, G., Takemura, T., Zhang, H., 2013. Chapter 8 Anthropogenic and Natural Radiative Forcing. IPCC 2013 Assessment Report 5th Climate Change - The Physical Science Basis, the Intergovernmental Panel on Climate Change [Stocker, T.F., D. Qin, G.-K. Plattner, M. Tignor, S.K. Allen, J. Boschung, A. Nauels, Y. Xia, V. Bex and P.M. Midgley (eds.)]. Cambridge University Press, Cambridge, United Kingdom and New York, NY, USA.

Nusselt, W., 1916. Die Oberflachenkondensation des wasserdampfes., *Veeines Dtsch. Ingenieure*, 60 (27) 541-546.

O'Doherty, S., Rigby, M., Mühle, J., Ivy, D.J., Miller, B.R., Young, D., Simmonds, P.G., Reimann, S., Vollmer, M.K., Krummel, P.B., Fraser, P.J., Steele, L.P., Dunse, B., Salameh, P.K., Harth, C.M., Arnold, T., Weiss, R.F., Kim, J., Park, S., Li, S., Lunder, C., Hermansen, O., Schmidbauer, N., Zhou, L.X., Yao, B., Wang, R.H.J., Manning, A., Prinn, R.G., 2014. Global emissions of HFC-143a (CH3CF3) and HFC-32 (CH2F2) from in situ and air archive atmospheric observations. *Atmos. Chem. Phys. Discuss*., 14, 6471-6500.

Perkins, R.A., Huber, M.L., 2011. Measurement and Correlation of the Thermal Conductivity of 2,3,3,3-Tetrafluoroprop-1-ene (R1234yf) and trans-1,3,3,3-Tetrafluoropropene (R1234ze(E)). *J. Chem. Eng. Data*, 56 (12) 4868-4874.

Ribatski, G., Jabardo, J.M.S., 2003. Experimental study of nucleate boiling of halocarbon refrigerants on cylindrical surfaces. *Int. J. Heat Mass Transf.*, 46, 4439-4451.

Shi, M.H., Ma, J., Wang, B.X., 1993. Analysis on hysteresis in nucleate pool boiling heat transfer. *Int. J. Heat Mass Transf.*, 36 (18) 4461-4466.

Stephan, K., Abdelsalam, M., 1980. Heat-transfer correlations for natural convection boiling. *Int. J. Heat Mass Transf.*, 23 (1) 73-87.

Tanaka, K., Higashi, Y., 2013. Surface Tensions of trans-1,3,3,3-Tetrafluoropropene and trans-1,3,3,3-Tetrafluoropropene +Difluoromethane Mixture. *J. Chem. Eng. Japan*, 46, 371-375.

Taylor, J.R., 1997. An introduction to error analysis, second ed. University science book, 73-77.

Velders, G.J.M., Fahey, D.W., Daniel, J.S., McFarland, M., Andersen, S.O., 2009. The large contribution of projected HFC emissions to future climate forcing. *Proc. Natl. Acad. Sci. U.S.A.*, 106, 10949-10954.

Velders, G.J.M., Ravishankara, R., Miller, M.K., Molina, M.J., Alcamo, J., Daniel, J.S., Fahey, D.W., Montzka, S., Reimann, S., 2012. Preserving Montreal Protocol Climate Benefits by Limiting HFCs. *Science*, 335, 922–923.

Wamsler, F., 1911. Die Wärmeabgabe geheizter Körper an Luft. *Ver Deut Ing Forschunash*: 98-99.

Yung, D., Lorenz, JJ., Ganic, E.N., 1980, Vapour/Liquid Interaction and Entrainment in Falling Film Evapourations, *Trans ASME*, *J. Heat Trans.*, 102 (1) 20-25.

Hodnebrog, Ø., Etminan, M., Fuglestvedt, J.S., Marston, G., Myhre, G., Nielsen, C.J., Shine, K.P., Wallington, T.J., 2013. Global warming potentials and radiative efficiencies of halocarbons and related compounds: A comprehensive review. Rev. Geophys. 51, 300-378.

Orkin, V.L., Martynova, L.E., Kurylo, M.J., 2014. Photochemical Properties of trans -1-Chloro-3,3,3-trifluoropropene (trans -CHCl═CHCF3): OH Reaction Rate Constant, UV and IR Absorption Spectra, Global Warming Potential, and Ozone Depletion Potential. *J. Phys. Chem.*, A118, 5263-5271.

Patten, K.O., Wuebbles, D.J., 2010. Atmospheric lifetimes and Ozone Depletion Potentials of trans-1-chloro-3,3,3-trifluoropropylene and trans-1,2-dichloroethylene in a three-dimensional model. Atmos. Chem. Phys. 10, 10867-10874.

Vollmer, M.K., Reimann, S., Hill, M., Brunner, D., 2015. First Observations of the Fourth Generation Synthetic Halocarbons HFC-1234yf, HFC-1234ze(E), and HCFC-1233zd(E) in the Atmosphere. *Environ. Sci. Technol.*, 49, 2703-2708.

Figure Captions

Figure 1 Experimental setup.
(a) water and refrigerant circuits (b) structure of the test section

Figure 2 Change in HTC with advance purification.

Figure 3 Variation in HTC versus wall subcool of low-GWP refrigerants.

Figure 4 Dimensionless condensation HTC of tested refrigerants.

Figure 5 Comparison of HTC between conventional and new low-GWP refrigerants.
(a) R134a and R1234ze(E) (b) R245fa, R1234ze(Z) and R1233zd(E)

Figure 6 Condensate behavior of R1234ze(E), R1234ze(Z), and R1233zd(E).
(a) R1234ze(E) Ref = 30, K = 0.008 (b) R1234ze(E) Ref = 101, K = 0.028 (c) R1234ze(E) Ref = 229, K = 0.068
(d) R1234ze(Z) Ref = 32, K = 0.010 (e) R1234ze(Z) Ref = 99, K = 0.028 (f) R1234ze(Z) Ref = 231, K = 0.069
(g) R1233zd(E) Ref = 33, K = 0.015 (h) R1233zd(E) Ref = 101, K = 0.043 (i) R1233zd(E) Ref = 135, K = 0.061

Figure 7 Condensate wavelengths of various refrigerants.

Figure 8 Hysteresis at nucleate boiling inception.

Figure 9 Visualization of results for the data plotted in Fig. 2.
(a) increasing at 5 kWm-2 (b) increasing at 15 kWm-2 (c) increasing at 20 kWm-2 (d) decreasing at 12 kWm-2

Figure 10 Boiling HTC as a function of heat flux
(a) at 10 °C (b) at 40 °C (c) at 60 °C

Figure 11 Bubble formation of low-GWP refrigerants on the horizontal plain tube.
(a) R134a at 20 ºC (p_{red} = 0.14) and 20 kWm^{-2}, α = 5.45 kWm^{-2}K^{-1}
(b) R1234ze(E) at 20 ºC (p_{red} = 0.12) and 20 kWm^{-2}, α = 4.21 kWm^{-2}K^{-1}
(c) R245fa at 20 ºC (p_{red} = 0.03) and 20 kWm^{-2}, α = 2.00 kWm^{-2}K^{-1}
(d) R1234ze(Z) at 20 ºC (p_{red} = 0.04) and 20 kWm^{-2}, α = 2.46 kWm^{-2}K^{-1}
(e) R1233zd(E) at 20 ºC (p_{red} = 0.03) and 20 kWm^{-2}, α = 1.66 kWm^{-2}K^{-1}
(f) R1234ze(Z) at 60 ºC (p_{red} = 0.15) and 20 kWm^{-2}, α = 4.87 kWm^{-2}K^{-1}.

Figure 12 Nucleation site density and bubble departure diameter.
Figure 13 Procedure to count the nucleation site

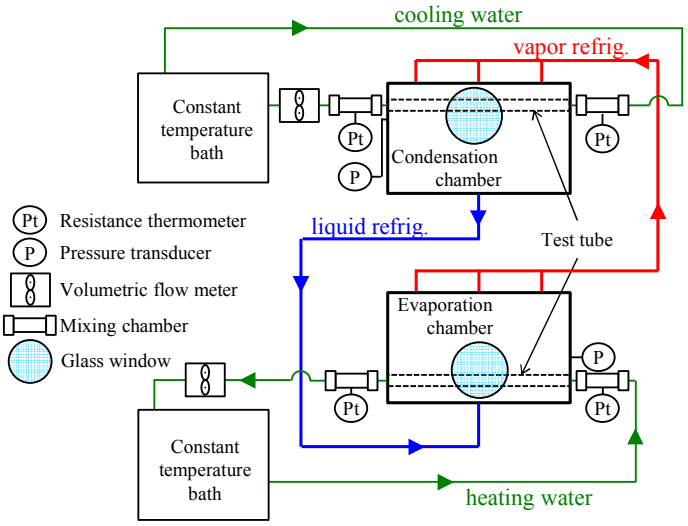

(a) water and refrigerant circuits

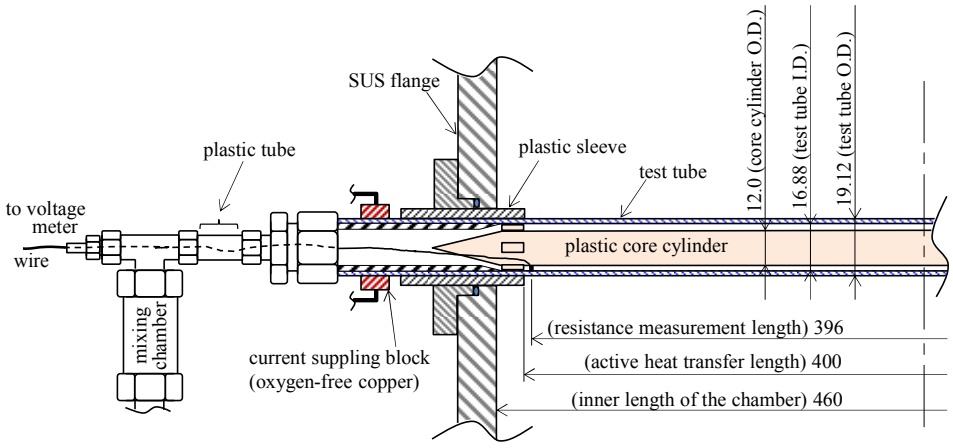

(b) structure of the test section

Figure 1 Experimental setup.

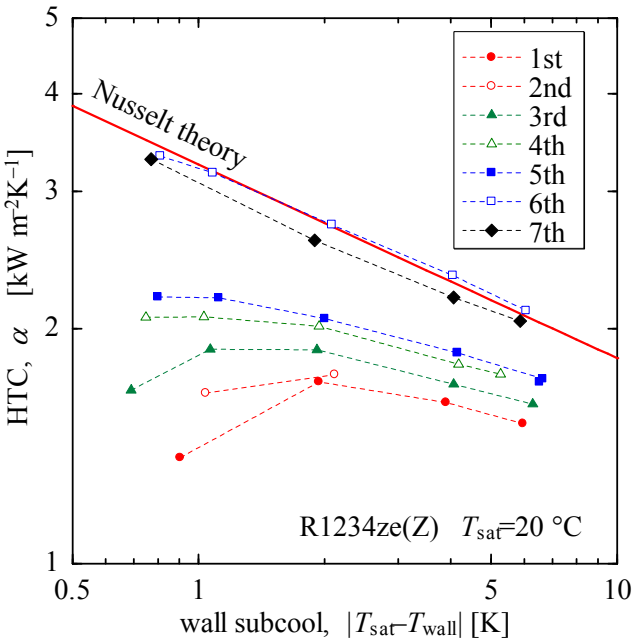

Figure 2 Change in HTC with advance purification.

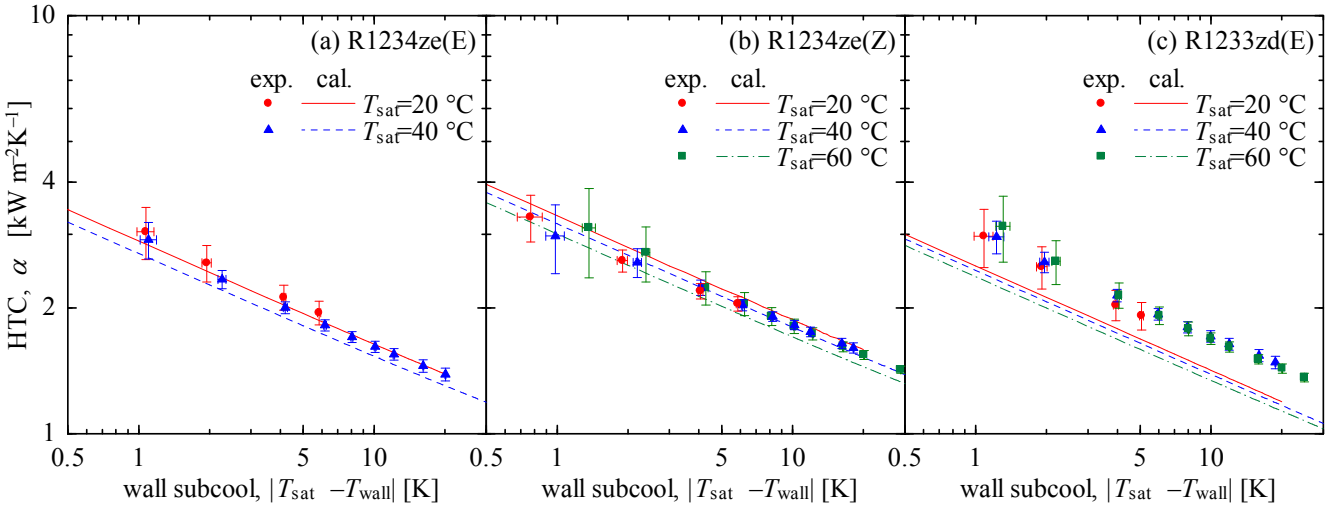

Figure 3 Variation in HTC versus wall subcool of low-GWP refrigerants.

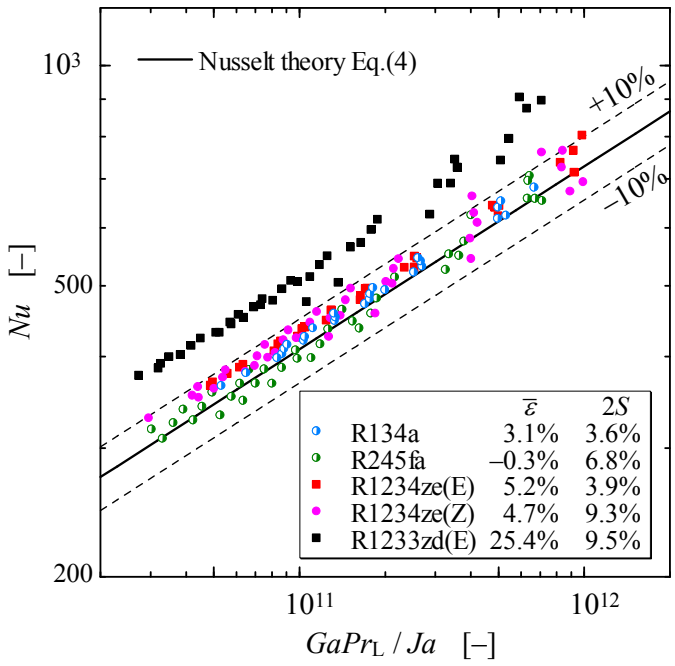

Figure 4 Dimensionless condensation HTC of tested refrigerants.

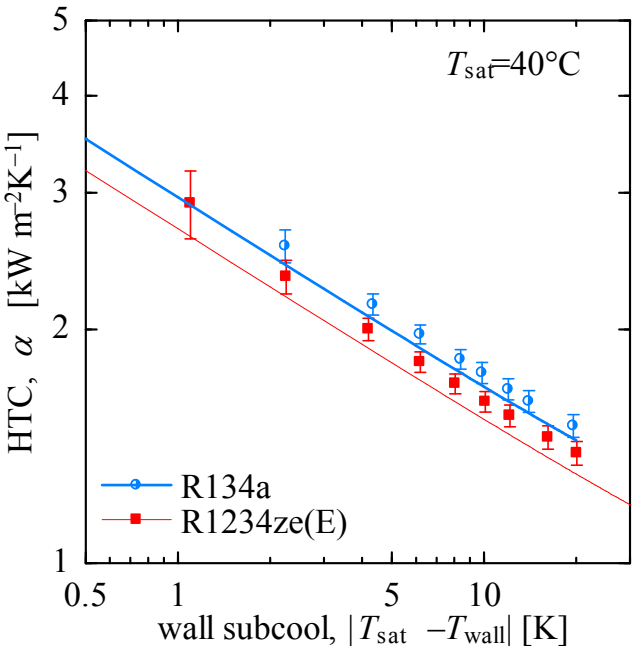

(a) R134a and R1234ze(E)

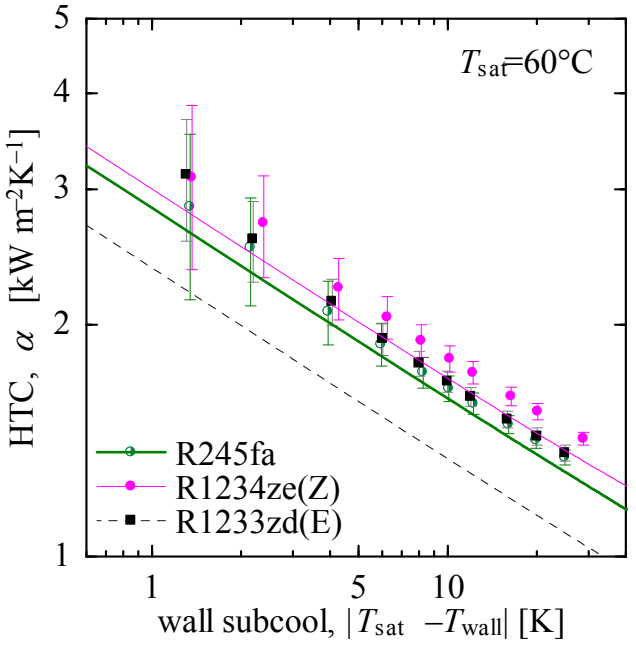

(b) R245fa, R1234ze(Z) and R1233zd(E)

Figure 5 Comparison of HTC between conventional and new low-GWP refrigerants.

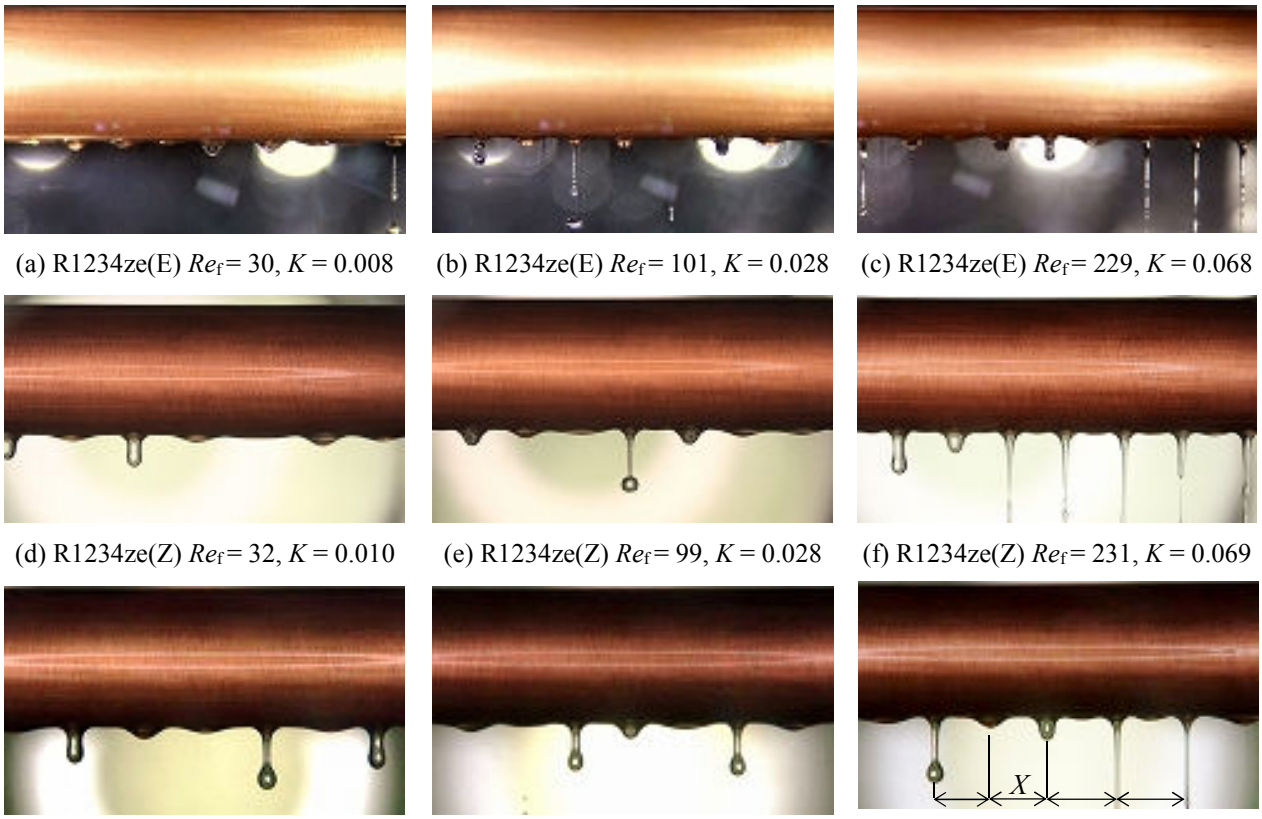

(a) R1234ze(E) Re_f= 30, K = 0.008 (b) R1234ze(E) Re_f= 101, K = 0.028 (c) R1234ze(E) Re_f= 229, K = 0.068

(d) R1234ze(Z) Re_f= 32, K = 0.010 (e) R1234ze(Z) Re_f= 99, K = 0.028 (f) R1234ze(Z) Re_f= 231, K = 0.069

(g) R1233zd(E) Re_f= 33, K = 0.015 (h) R1233zd(E) Re_f= 101, K = 0.043 (i) R1233zd(E) Re_f= 135, K = 0.061

Figure 6 Condensate behavior of R1234ze(E), R1234ze(Z), and R1233zd(E).

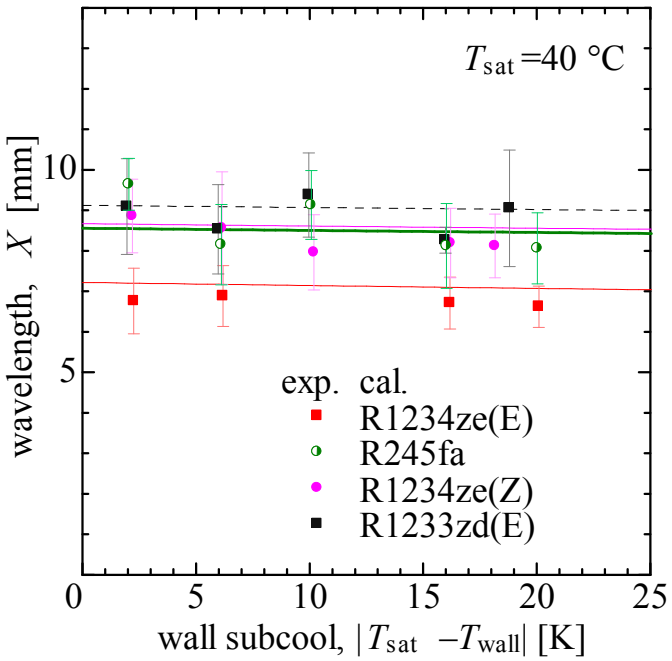

Figure 7 Condensate wavelengths of various refrigerants.

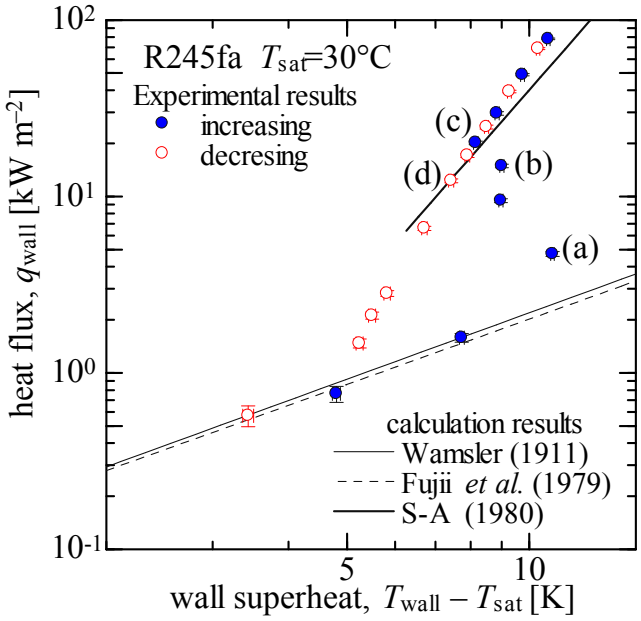

Figure 8 Hysteresis at nucleate boiling inception.

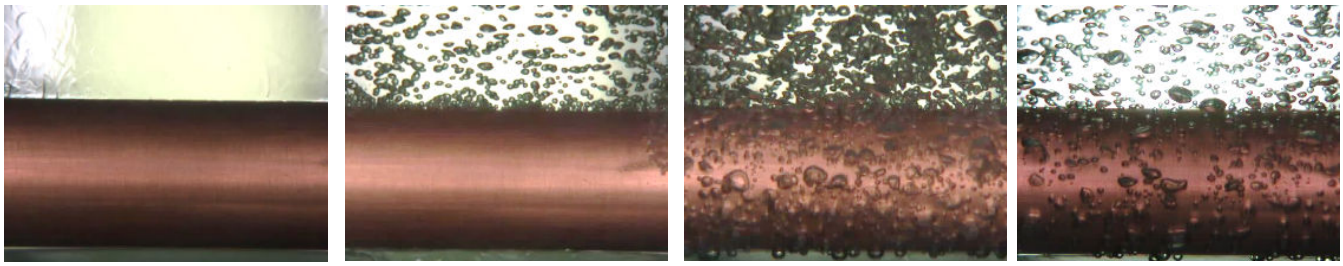

(a) increasing at 5 kWm^{-2} (b) increasing at 15 kWm^{-2} (c) increasing at 20 kWm^{-2} (d) decreasing at 12 kWm^{-2}

Figure 9 Visualization of results for the data plotted in Fig. 2.

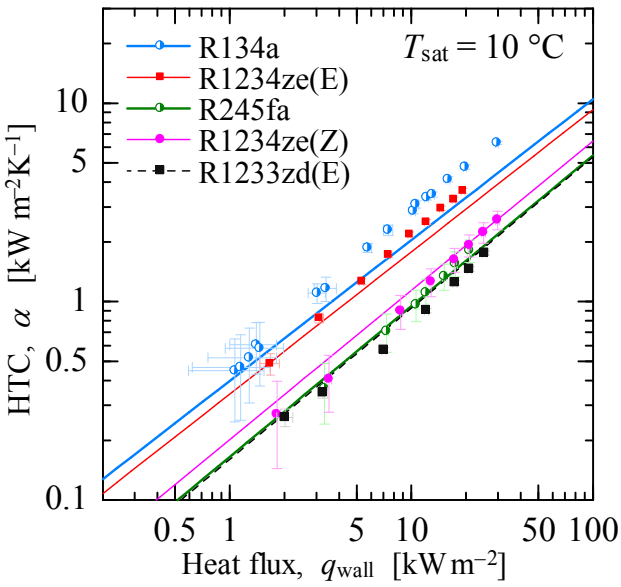

(a) at 10 °C

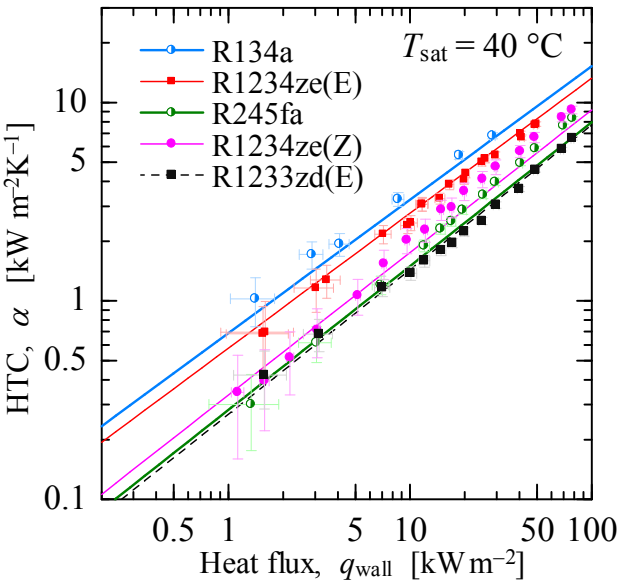

(b) at 40 °C

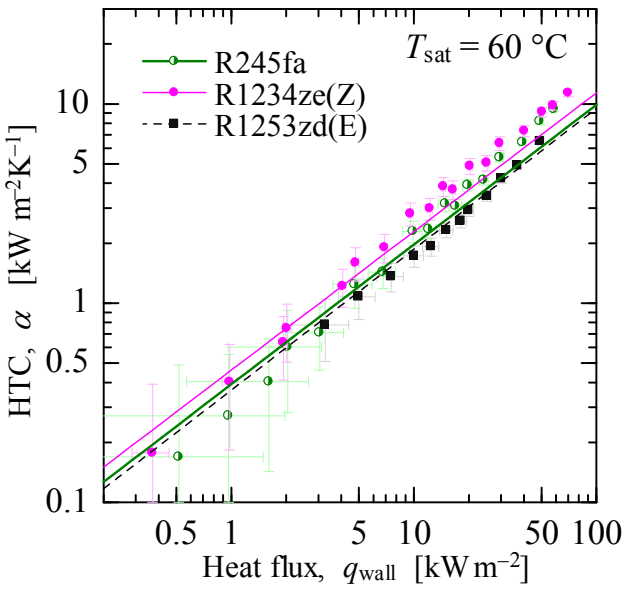

(c) at 60 °C

Figure 10 Boiling HTC as a function of heat flux

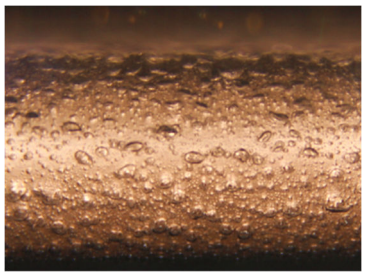

(a) R134a at 20 ºC (p_{red} = 0.14) and 20 kWm^{-2}, α = 5.45 kWm^{-2}K^{-1}

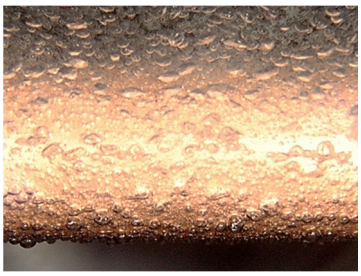

(b) R1234ze(E) at 20 ºC (p_{red} = 0.12) and 20 kWm^{-2}, α = 4.21 kWm^{-2}K^{-1}

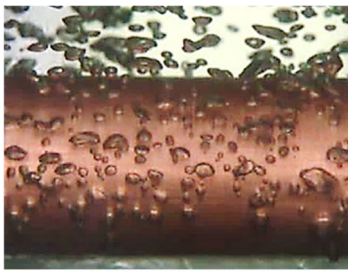

(c) R245fa at 20 ºC (p_{red} = 0.03) and 20 kWm^{-2}, α = 2.00 kWm^{-2}K^{-1}

(d) R1234ze(Z) at 20 ºC (p_{red} = 0.04) and 20 kWm^{-2}, α = 2.46 kWm^{-2}K^{-1}

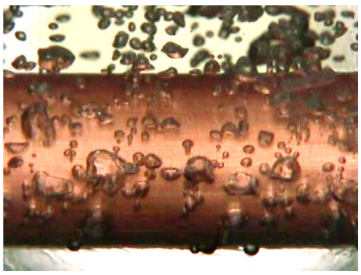

(e) R1233zd(E) at 20 ºC (p_{red} = 0.03) and 20 kWm^{-2}, α = 1.66 kWm^{-2}K^{-1}

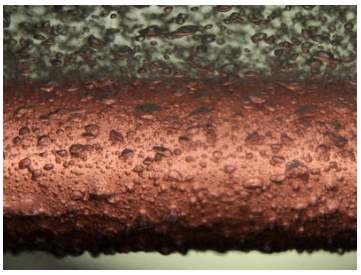

(f) R1234ze(Z) at 60 ºC (p_{red} = 0.15) and 20 kWm^{-2}, α = 4.87 kWm^{-2}K^{-1}

Figure 11 Bubble formation of low-GWP refrigerants on the horizontal plain tube.

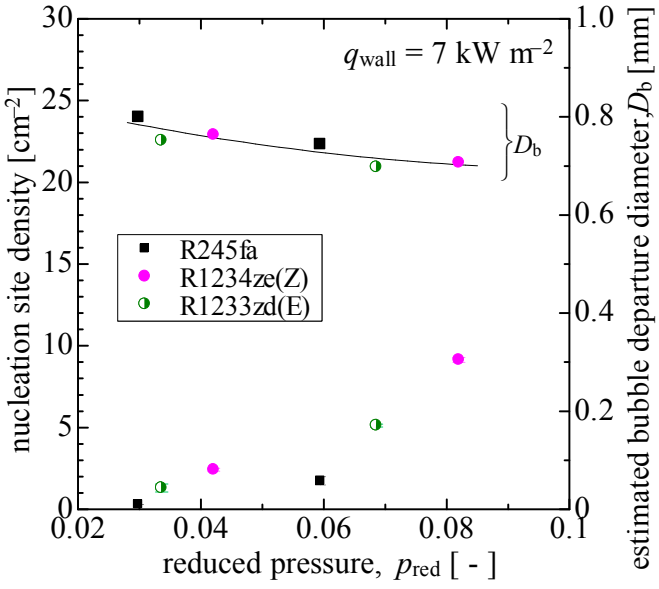

Figure 12 Nucleation site density and bubble departure diameter.

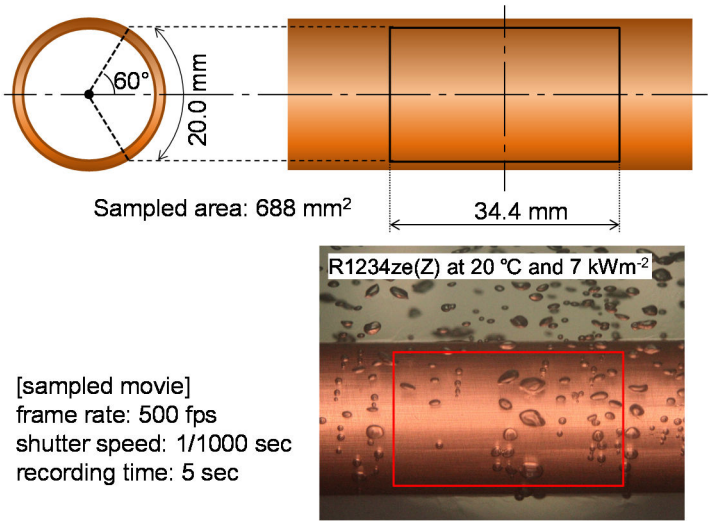

Figure 13 Procedure to count the nucleation site

Table 1 Experimental conditions.

Outer diameter of the tube	D_o	19.12	mm
Inner diameter of the tube		16.88	mm
Active heat transfer length	L	400	mm
Surface roughness or the tube	R_a	0.41 (condensation) 0.39 (boiling)	μm
	R_p	1.33 (condensation) 1.18 (boiling)	μm
Test refrigerants		R134a, R1234ze(E), R245fa, R1234ze(Z), R1233zd(E)	—
Temperature change of water		3	K
		for condensation	
Saturation temperature	T_{sat}	20 ~ 60	°C
Degree of wall subcool		0.77 ~ 28.81	K
Heat flux	q_{wall}	3.06 ~ 40.99	kW m^{-2}
		for pool boiling	
Saturation temperature	T_{sat}	10 ~ 60	°C
Degree of wall superheat		1.19 ~ 9.17	K
Heat flux	q_{wall}	0.73 ~ 80.13	kW m^{-2}

Table 2 Thermodynamic and transport properties of test refrigerants.

Refrigerant	R134a	R1234ze(E)	R245fa	R1234ze(Z)	R1233zd(E)
ODP	0	0	0	0	0.00034 [8] 0.00050 [9]
GWP_{100}	1300 [1)3)]	<1 [1)3)] up to 7.5 [2)]	858 [1)3)]	<1 [1)3)]	1 [1)] 4 to 14 [2)]
safety classification [4)]	A1	A2L [4)]	B1	A2L [5)] (expected)	A1 [7)]
P_{crit} [MPa]	4.059	3.635	3.651	3.533	3.571
T_{crit} [°C]	101.1	109.4	154.0	150.1	166.5
NBP [°C] *	-26.1	-19.0	15.1	9.7	18.3
h_{LV} [kJ kg^{-1}] **	163.0	154.8	181.14	196.36	183.1
ρ_L / ρ_V [kg m^{-3}] **	1146.7 / 50.09	1111.5 / 40.64	1296.7 / 14.12	1180.7 / 14.14	1225.6 / 11.67
λ_L [mW m^{-1}K^{-1}] **	74.7	69.2	83.36	84.64	71.10
μ_L [μPa·s] **	161.5	167.0	328.58	201.3	388.05
σ [mN m^{-1}] **	6.11	6.96	11.73	10.94 [6)]	12.62 [6)]

* Normal Boiling Point, ** at a saturation point of 40 °C

1) Hodnebrog et al. (2013), 2)Vollmer et al. (2015), 3) Myhre et al. (2013), 4) ASHRAE STANDARD (2011), 5) Koyama et al. (2013), 6) Kondou et al. (2015), 7) ASHRAE STANDARD (2015), 8) Patten et al. (2010), 9) Orkin et al. (2014)

Table 3 Measurement uncertainty.

Parameter		instrument / method	uncertainty
tube diameter	D_o	slide caliper	±0.1 mm
heat transfer length	L	scale	±1 mm
water temperature	T_{H2O}	Pt resistance thermometer	±0.05 K
volumetric flow rate of water	V_{H2O}	gear-type volumetric flow meter	±0.5% of reading
pressure	P	absolute pressure transducer	±0.19 kPa
tube wall temperature	T_{wall}	electric resistance method	±0.078 K

Table 4 Contribution of thermophysical properties on condensation HTC.

	R134a	R1234ze(E)		R245fa	R1234ze(Z)		R1233zd(E)	
	at T_{sat} = 40 °C and $\|T_{sat} - T_{wall}\|$ = 10 K			at T_{sat} = 60 °C and $\|T_{sat} - T_{wall}\|$ = 10 K				
$\lambda_L^{0.75}$	0.146	0.137	(94%)	0.148	0.150	(101%)	0.132	(89%)
$[\rho_L(\rho_L-\rho_V)]^{0.25}$	33.81	33.31	(99%)	35.21	33.55	(95%)	34.30	(97%)
$h_{LV}^{0.25}$	20.09	19.84	(99%)	20.24	20.65	(102%)	20.35	(101%)
$\mu_L^{-0.25}$	8.73	8.66	(99%)	7.79	8.28	(106%)	7.46	(96%)
α, HTC	1.68	1.53	(91%)	1.60	1.67	(104%)	1.34	(84%)

†Parenthesized percentages are relative values to the properties of R134a or R245fa.

Table 5 Relative bias and standard deviation of the predicted HTC from the experimental HTC.

	Stephan-Abdelsalam (1980)		Ribatski-Jabardo (2003)		Jung *et al.* (2003)		Gorenflo *et al.* (2010)	
Refrigerant	$\overline{\varepsilon}$ [%]	S [%]	$\overline{\varepsilon}$ [%]	S [%]	$\overline{\varepsilon}$ [%]	S [%]	$\overline{\varepsilon}$ [%]	S [%]
R134a	42.5	19.9	16.4	19.2	6.2	21.7	-7.8	21.7
R1234ze(E)	3.5	16.9	0.2	15.0	-15.4	20.4	-26.5	20.6
R245fa	-1.6	11.6	8.2	15.7	4.7	20.6	-6.6	9.0
R1234ze(Z)	30.7	16.9	8.9	16.8	4.8	20.9	11.4	22.6
R1233zd(E)	-14.7	8.7	-1.9	10.4	19.1	16.0	12.1	35.3
overall	10.2	24.8	5.5	16.4	3.1	23.2	-2.7	27.7